

Na₉Bi₅Os₃O₂₄: A Unique Diamagnetic Oxide Featuring a Pronouncedly Jahn-Teller Compressed Octahedral Coordination of Osmium(VI)

Gohil S. Thakur,^{†‡} Hans Reuter,[‡] Alexey V. Ushakov,^{||} Gianpiero Gallo,[¶] Jürgen Nuss,[¶] Robert E. Dinnebier,[¶] Sergey V. Streltsov,^{||} Daniel I. Khomskii,[§] and Martin Jansen^{¶*}

[†] Max Planck Institute for Chemical Physics of Solids, Nöthnitzerstr. 40, 01187 Dresden, Germany

[‡] Faculty of Chemistry and Food Chemistry, Technical University, 01069 Dresden, Germany

[‡] Institute for Chemistry of new Materials, University of Osnabrück, Barbarastraße 7, 49069 Osnabrück, Germany

^{||} M. N. Mikheev Institute of Metal Physics, Ural Branch of Russian Academy of Sciences, 620002 Ekaterinburg, Russia

[¶] Max Planck Institute for Solid State Research, Heisenbergstr. 1, 70569 Stuttgart, Germany

[§] II Physikalisches Institut, Universität zu Köln, Zùlpicher Str. 77, 50937 Köln, Germany

KEYWORDS. *Jahn-Teller compression, spin-orbit coupling, multinary osmate, hydrothermal synthesis.*

ABSTRACT: The Jahn-Teller (JT) theorem constitutes one of the most popular and stringent concepts, applicable to all fields of chemistry. In open shell transition elements chemistry and physics, $3d^4$, $3d^9$, and $3d^7$ (low-spin) configurations in octahedral complexes serve as particular illustrative and firm examples, where a striking change (“distortion”) in local geometry is associated to a substantial reduction of electronic energy. However, there has been a lasting debate, almost of a historical dimension, about the fact that the octahedra are found to exclusively elongate, (at least for e_g electrons). Against this background, the title compound displays two marked features, (1) the octahedron of oxygen atoms around Os⁶⁺ with d^2 configuration is drastically compressed, in contrast to the standard JT expectations, and (2) the splitting of the t_{2g} set of $5d$ orbitals induced by this compression is extreme, such that a diamagnetic ground state results. What we see is obviously a Jahn-Teller distortion resulting in a *compression* of the respective coordinating octahedron and acting on the t_{2g} set of orbitals. Both these issues are unprecedented. Noteworthy, the splitting into a lower d_{xy} (hosting two d electrons with opposite spin) and two higher d_{xz} and d_{yz} orbitals is so large that for the first time ever the Hund’s coupling for t_{2g} electrons is overcome. We show that these effects are not forced by structural frustration, the structure offers sufficient space for Os to shift the apical oxygen atoms to a standard distance. Local electronic effects appear to be responsible, instead. The relevance of these findings is far reaching, since they provide insights in the hierarchy of perturbations defining ground states of open shell electronic systems. The four component system studied here, offers substantially more structural and compositional degrees of freedom, such that a configuration could form that enables Os⁶⁺ to adopt its apparently genuine diamagnetic ground state.

INTRODUCTION

Dealing with multitudes of particles constitutes an inescapable and major challenge in chemistry, even within the framework of the Born-Oppenheimer approximation. While for molecular species the numbers of atoms involved are finite, they are virtually infinite for extended solids. In coping with the task of structuring and classifying chemical knowledge for purposes of e.g. communication, teaching, understanding or planning of chemical research the enormous richness of empirical and computational results need to be cast into comprehensible concepts.¹ Along the most popular of such approaches, one tries to structure observations, and even to derive cause-effect relationships, by breaking down collective properties into additive increments. Prominent examples are atomic radii (from distances),² electronegativity (from shortening of covalent bonds due to polarity),³ oxidation states (assigning charges by systematic definition),⁴ or the reverse, bulk diamagnetic response of a compound (from calculated increments).⁵ Such procedures are most reliable for compounds consisting of only two different elements, making it easier to separate the individual contributions of the constituting atoms. However, as a distinct disadvantage of such binaries the degrees of freedom in evolving different compositions, structures, bonding schemes and properties are substantially limited. With respect to both these issues, the opposite holds true for multinary compositions, and the individual constituting atom types are less constrained in striving for their respective pertinent preferred configurations.

Here we report on an illustrative example of a novel four-component oxide Na₉Bi₅Os₃O₂₄ in which the additional degrees

of freedom have enabled a complex composition and a singular crystal structure where the constituents Na, Bi, Os, and O come close to their characteristic structure and bonding properties. As a surprising result, although containing Os⁶⁺ with a $5d^2$ electron configuration, the compound is diamagnetic and exhibits a drastically compressed octahedron around osmium, which causes an exceptionally strong crystal field splitting of the t_{2g} levels thus lifting the degeneracy of unequally occupied orbitals according to a Jahn-Teller (JT) effect. This finding is very special in another, more general respect. In known solids the transition metal (TM) ions with partially-filled t_{2g} levels always obey the first Hund’s rule, *i.e.* electrons are arranged such that the maximum S results. We are not aware of any exception of this rule for t_{2g} shells in extended solids. In one incident, La₄Ru₂O₁₀, it was initially suggested that Ru⁴⁺ has an S = 0 ground state.⁶ This was challenged later, and shown that the nonmagnetic character of this system is due to the formation of singlet Ru dimers (“molecules in solids”).⁷ In our case, as we show below, Os⁶⁺ ($5d^2$) really has a singlet ground state with S = 0, strongly violating the first Hund’s rule. This particular configuration may form because of a synergetic action of weaker structural matrix effects of the many-component material and a strong local JT effect, seen for the first time to act on the t_{2g} levels of an octahedral complex and to induce a compression.

EXPERIMENTAL SECTION

Synthesis and crystal growth. Intimately mixed powders of Bi₂O₃ (0.0777 g, 0.5 mol, Alfa Aesar 99.9 %) OsO₂ (0.1482, 2 mol, Alfa Aesar 99.5%) and Na₂O₂ (0.078 g, 3 mol, homemade)

to which 0.5 ml of water was added (1 ml of 5 M NaOH solution can be used instead of Na₂O₂), were heated under high oxygen pressure and at high temperature. The solid starting materials were ground in an Ar filled dry glove box and transferred into a gold finger welded at one end. Water was added dropwise outside the glove box immediately before crimping the tube from the top end and placing it in a steel autoclave. The autoclave was tightly sealed after approximately 11.2 ml of liquid oxygen was condensed in it. This amount of oxygen would generate a pressure of around 350 MPa at 773 K. The reaction was carried out for 4 days in a vertical furnace before cooling it naturally. The product was vacuum filtered inside a fume hood and rinsed with distilled water first and subsequently with ethanol. Black reflective hexagonal blocks or thick plates were obtained which were further cleaned and separated by ultra-sonication under ethanol. Crystals of maximum dimensions of up to 1×1×1 mm³ could be obtained. A white powdery layer on the crystals appears after a few weeks of exposure to moist air, while the powder diffraction pattern did not seem to change. The product was stored in a glove box.

Caution: Under the given conditions, reaction involving osmium generates highly toxic OsO₄, hence, care must be taken during the release of pressure inside the fume hood. Before fetching the product, the opened autoclave was left for several hours inside the fume hood to allow OsO₄ to escape completely. Use of proper PPE (eye protection, respirator as well as latex gloves) is necessary.

Chemical analyses. Semiquantitative analysis was performed by scanning electron microscopy-energy dispersive analysis by X-rays (SEM-EDAX). Many crystals from different batches were examined and the data averaged to obtain the metal composition, see Figure S1 in supporting information (SI). Wet chemical analyses of the metal contents were performed by Mikroanalytisches Labor Pascher, An der Pulvermühle 1, D-53424 Remagen, Germany (microwave pressure digestion with HNO₃/HF/HCl; Bi and Os determined by ICP-OES, Na by AAS). Two different runs on the same batch of sample were averaged to obtain the atomic fraction. The results are presented Table S1 in SI.

Thermogravimetric (TGA) analysis of the collected single crystals was carried out on a Netzsch STA 449 C analyzer. About 30 mg of the sample was placed in a corundum crucible, which was heated and subsequently cooled at a rate of 5 K min⁻¹ in the range of 300–1273 K under dynamic argon flow, see Figure S2 in SI.

Physical properties. Susceptibility of loose single crystals was measured in applied magnetic fields $\mu_0H = 0.1, 1.0$ and 3.5 T and in the temperature range between 2 and 350 K in a MPMS-XL7 magnetometer (Quantum Design). Temperature dependent resistivity in the temperature range, $T = 150$ –400 K was measured on a block-like single crystal of dimension approximate dimensions 1 × 0.8 × 0.7 mm³ using a two-probe method in a PPMS instrument (Quantum Design).

Crystal structure determination. The determination of the crystal structure by X-ray diffraction did not proceed straight forwardly and required to employ both powder and single crystal techniques in an alternating fashion.

X-Ray Powder Diffraction (XRPD) measurements were performed using a Stoe Transmission Powder Diffraction System (STADI-P, STOE & CIE, Ge(111) Johansson-type monochromator, AgK α_1 radiation ($\lambda = 0.55941$ Å)) that was equipped

with an array of three linear position-sensitive MYTHEN 1K detectors from Dectris Ltd. of approximately 18° 2 θ opening angle each. The finely powdered sample of Na₉Bi₅Os₃O₂₄ was placed in a glass capillary of 0.3 mm (Hilgenberg glass No. 14) and spun during measurement for improving particle statistics. The measurement in the range from 1.0 – 111.0° 2 θ with a step width of 0.015° 2 θ took 3 hrs (Figure 1). For indexing of the powder pattern of Na₉Bi₅Os₃O₂₄ at $T = 298$ K, the program TOPAS version 6 (Bruker-AXS, 2018)⁸ was used, leading to a hexagonal unit cell with parameters of $a = 9.8264(1)$ and $c = 12.8573(2)$ Å ($V = 1075.16(3)$ Å³). The most probable space groups were determined as $P31c$ (159), $P\bar{3}1c$ (163), $P6_3mc$ (186), $P\bar{6}2c$ (190), and $P\bar{6}_3/mc$ (194) from the observed extinction rules, out of these $P\bar{6}2c$ was confirmed after structure determination. Structure determination of Na₉Bi₅Os₃O₂₄ was performed in all possible space groups by the method of Charge Flipping⁹, supported by the inclusion of the tangent formula¹⁰ as implemented in TOPAS.⁸ The positions of the heavier atoms (Bi, Os) and some candidate for the sodium atoms were found for several space groups but with a clear preference for $P\bar{6}2c$. The space group assumed and the heavy atom structure were confirmed using single crystal X-ray diffraction data, which also enabled to identify the missing light atoms. These final results comply well with the PXRD, as was validated by Rietveld refinement using the TOPAS program. An overall isotropic temperature factor was refined. The profiles related to the final Rietveld refinement are shown in Figure 1. The weighted profile R-factor is 3.55 %, the Bragg R-factor is 1.91 %, with a goodness of fit of 2.26. The atomic coordinates are given in Table S2 and a selection of intramolecular distances and angles is given in Table S3 in SI.

Crystals suitable for single-crystal X-ray diffraction were selected under highly viscous oil, and mounted with grease on a loop made of Kapton foil (Micromounts™, MiTeGen, and Ithaca, NY). Diffraction data were collected at 298 K with a SMART APEXII CCD X-ray diffractometer (Bruker AXS, Karlsruhe, Germany), using graphite-monochromated Mo-K α radiation. Reflection intensities were integrated with the SAINT subprogram in the Bruker Suite software,¹¹ a multi-scan absorption correction was applied using SADABS,¹² and the structure was refined by full-matrix least-square fitting with the SHELXTL software package.^{13,14} According to the systematic reflection condition $hh\bar{2}hl$ only present for $l = 2n$, trigonal space groups $P31c$ (159), $P\bar{3}1c$ (163), and hexagonal space groups $P6_3mc$ (186), $P\bar{6}2c$ (190) and $P6_3/mmc$ (194) have been checked for structure solution, however, any structure solution method of the SHELXS package failed. The heavy-element positions from powder solutions in the non-centrosymmetric space group $P\bar{6}2c$ proved to be a suitable starting model for resolving the complete structure via Difference Fourier analyses. Refinement with anisotropic thermal parameters for all atoms without applying any constraints converged easily. Crystal data and data collection details, positional and isotropic thermal parameters and bond distances, respectively, are given in Tables 1-3, the anisotropic thermal parameters in Table S4 in SI. The crystallographic data have been deposited at ICSD under CSD-No. 2063496.

Table 1. Crystal and structure refinement data for Na₉Bi₅Os₃O₂₄ from SCXRD.

Empirical formula	Na ₉ Bi ₅ Os ₃ O ₂₄
Formula weight [g/mol]	2206.41
T [K]	296(2)
Crystal system, space group	Hexagonal, $P\bar{6}2c$
a [Å]	9.8115(3)
c [Å]	12.8457(5)
V [Å ³]	1070.93(8)
Z, d _{calc} [g/cm ³]	2, 6.842
μ(MoKα) [mm ⁻¹]	58.944
F(000)	1868
2θ _{max}	70°
Reflections collected	75234
Reflections unique, R _{int}	1637, 0.0877
Data / restraints / parameters	1637 / 0 / 70
Goodness-of-fit on F ²	1.040
R ₁ , wR2 [I > 2σ(I)]	0.0208, 0.0529
R ₁ , wR2 [all data]	0.0268, 0.0567
Absolute structure parameter	-0.038(6)
Extinction coefficient	0.00102(6)
±Δ [eÅ ⁻³]	1.728/-3.396

Table 2: Atomic coordinates (× 10⁴) and equivalent isotropic displacement parameters (Å² × 10³) for Na₉Bi₅Os₃O₂₄ obtained from single crystal structure refinement. U_{eq} is defined as one third of the trace of the orthogonalized U_{ij} tensor.

Atom	site	x	y	z	U _{eq}
Os1	6h	6682(1)	9975(1)	2500	3.9(1)
Bi1	6g	6712(1)	10000	5000	4.5(1)
Bi2	4f	3333	6667	6051(1)	7.4(1)
Na1	2b	10000	10000	2500	17(1)
Na2	12i	2976(6)	9912(4)	3789(2)	13(1)
Na3	4f	3333	6667	3731(4)	16(1)
O1	6h	8035(11)	12028(12)	2500	10(1)
O2	6h	5648(8)	7895(11)	2500	10(1)
O3	12i	5336(5)	7486(6)	5037(3)	7.3(8)
O4	12i	5443(6)	10127(6)	3631(4)	8.1(9)
O5	12i	7987(7)	9862(7)	3703(4)	8.3(9)

Table 3. Selected bond distances for Na₉Bi₅Os₃O₂₄.

Atom pairs	Distance (Å)	Atom pairs	Distance (Å)
Os1-O2 (×1)	1.767(10)	Na1-O5 (×6)	2.457(5)
Os1-O1 (×1)	1.773(11)	Na2-O4 (×1)	2.335(7)
Os1-O4 (×2)	1.944(5)	Na2-O1 (×1)	2.406(9)
Os1-O5 (×2)	2.044(5)	Na2-O3 (×1)	2.440(6)
Bi1-O5 (×2)	2.129(5)	Na2-O5 (×1)	2.441(7)
Bi1-O3 (×2)	2.140(5)	Na2-O2 (×1)	2.480(8)
Bi1-O4 (×2)	2.191(5)	Na2-O3 (×1)	2.490(6)
Bi2-O3 (×3)	2.150(5)	Na3-O2 (×3)	2.396(6)
Bi2-O1 (×3)	2.937(5)	Na3-O3 (×3)	2.525(6)

Computational methods. We used the Vienna Ab-initio Simulation Package (VASP) and the generalized gradient approximation for DFT calculations.¹⁵ The on-site Coulomb repulsion U and Hund's intra-atomic exchange J_H parameters were chosen to be 1.1 and 0.5 eV, so that $U - J_H = 0.6$ eV.¹⁶ A 5×5×5 mesh in k -space was used. For simplicity we assumed ferromagnetic order (to avoid effects of magnetostriction). Crystal-field splitting parameters were obtained from non-magnetic DFT calculations (computing barycenters of corresponding bands) using Linearized Muffin-Tin Orbitals method.¹⁷

RESULTS AND DISCUSSION

Synthesis, chemical materials properties. Na₉Bi₅Os₃O₂₄ was obtained by reacting the binary constituent oxides at high oxygen pressure and hydrothermal conditions. Black reflective hexagonal blocks or thick plates were harvested after washing the product with water and rinsing with ethanol (Figure 1). Several crystals from different batches were quantitatively analyzed using SEM-EDX, which showed an approximate metal ratio of Na/Bi/Os = 3.1/1.8/1 (Figure S1 in SI). A composition of Na_{8.63}Bi_{4.81}Os_{3.0}O_{24.4} was estimated from ICP-OES and AAS analysis of the metal concentrations (see Table S1 in SI) basically confirming the composition obtained from EDAX. The compound starts decomposing in a stepwise manner at 600 K (See Figure S2 in SI) but the decomposition is not complete till 1273 K.

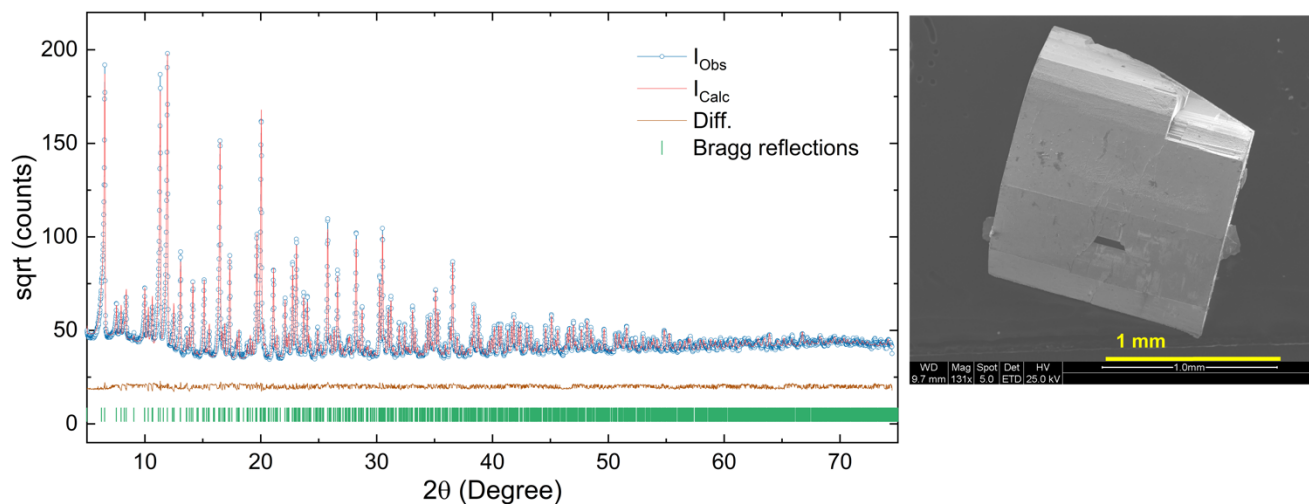


Figure 1. Rietveld fit to the powder X-ray diffraction pattern of $\text{Na}_9\text{Bi}_5\text{Os}_3\text{O}_{24}$. Blue, Red and brown lines are the observed, calculated and difference curve, respectively. The green vertical bars represent the allowed Bragg reflections. To the right is the electron microscopic image of a typical crystal.

The powder X-ray diffraction pattern was indexed and refined using the final atomic parameters from the single crystal structure determination as a starting model. No apparent impurity phase was observed in the powder pattern. Figure 1 shows the result of a Rietveld profile refinement, for more details see Supporting Information (SI), Tables S2 and S3.

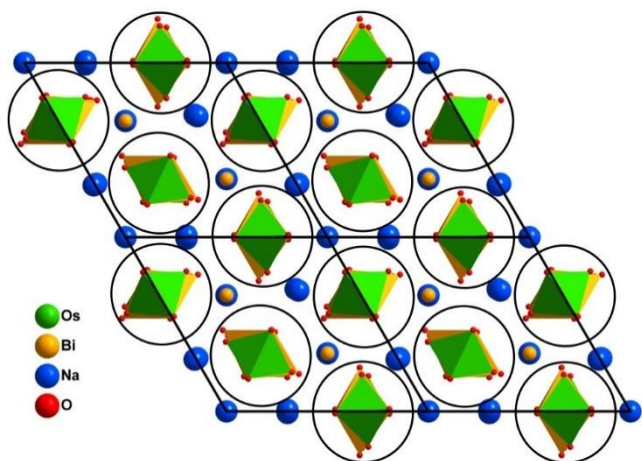


Figure 2. Projection of the crystal structure, view direction $[001]$, strands of alternating OsO_6 and BiO_6 octahedra are emphasized by black circles.

Crystal structure, description. From the structure and chemical formula it was deduced that osmium is hexavalent and bismuth is mixed-valent with three out of five (Bi^{1+}) being pentavalent and the remaining trivalent (Bi^{2+}). $\text{Na}_9\text{Bi}_5\text{Os}_3\text{O}_{24}$ exhibits a singular and peculiar crystal structure that cannot be related to any of the prominent aristotypes of typical oxide structure families. Here, for providing a comprehensive description, we resort to the tool of analyzing extended structures in terms of rod packings.^{18,19} As is emphasized in Figure 2, all secondary building units are quasi-1D and form chains extending in c direction

of the hexagonal crystal system. Strands of edge sharing octahedra, centered in an alternating fashion by Os^{6+} and Bi^{5+} , are dominating and constitute a precisely hexagonal rod packing. All oxygen atoms in the structure are attached to these chains. Positions and orientations of the latter generate columns of trigonal prisms around the threefold axes of the space group at $1/3$ $2/3$ z (1), $2/3$ $1/3$ z (2) and 0 0 z (3), while a fourth column of oxygen atoms around Na_2 is not subject to space group symmetry constraints. The individual rods are shown in Figure 3. The respective local coordinations for the chain of edge sharing octahedra show a typical pattern for Bi^{5+} , however, an extremely compressed octahedron around Os^{6+} , which is a conspicuous structural feature for this ion and is without precedent. Interestingly, the trigonal prisms of columns (1) and (2) are each occupied by trivalent Bi^{2+} and Na_3 in a pairwise alternating fashion, instead of simply alternating, which would be favorable for electrostatic reasons. The coordination polyhedra observed for these atoms are basically as expected. Bismuth(III) forms a trigonal pyramid with three short bonds, and three distinctly longer ones, in accord with the “active lone-pair” scenario.^{20,21} Na_3 as well shows common distances towards oxygen on average, however, is seemingly unforced in an off-center position. The trigonal strands around the origin of the unit cell comprise alternating filled, $(\text{Na}_1)\text{O}_6$, and empty regular trigonal prisms. Within the remaining chain, Na_2 is coordinated by six nearest oxygen atoms, forming a substantially distorted octahedron. These polyhedra are connected to chains oriented along $[001]$ via common edges $\text{O}_1\text{--O}_2$ and $\text{O}_3\text{--O}_3$, respectively. The rods are linked to form a three-dimensional framework, basically via the apical oxygen atoms of the Bi^{5+} and Os^{6+} octahedra. Now, the key role played by the distorted trigonal prisms around trivalent Bi^{2+} and Na_3 in controlling the bond length to the apical oxygen atoms is becoming evident: The particular sequence of Bi^{2+} and Na_3 is generating a breathing mode of the oxygen atoms reflected by small triangles between Bi^{2+} and Na_3 atoms and wider ones between each two subsequent Bi^{2+} and Na_3 , respectively.

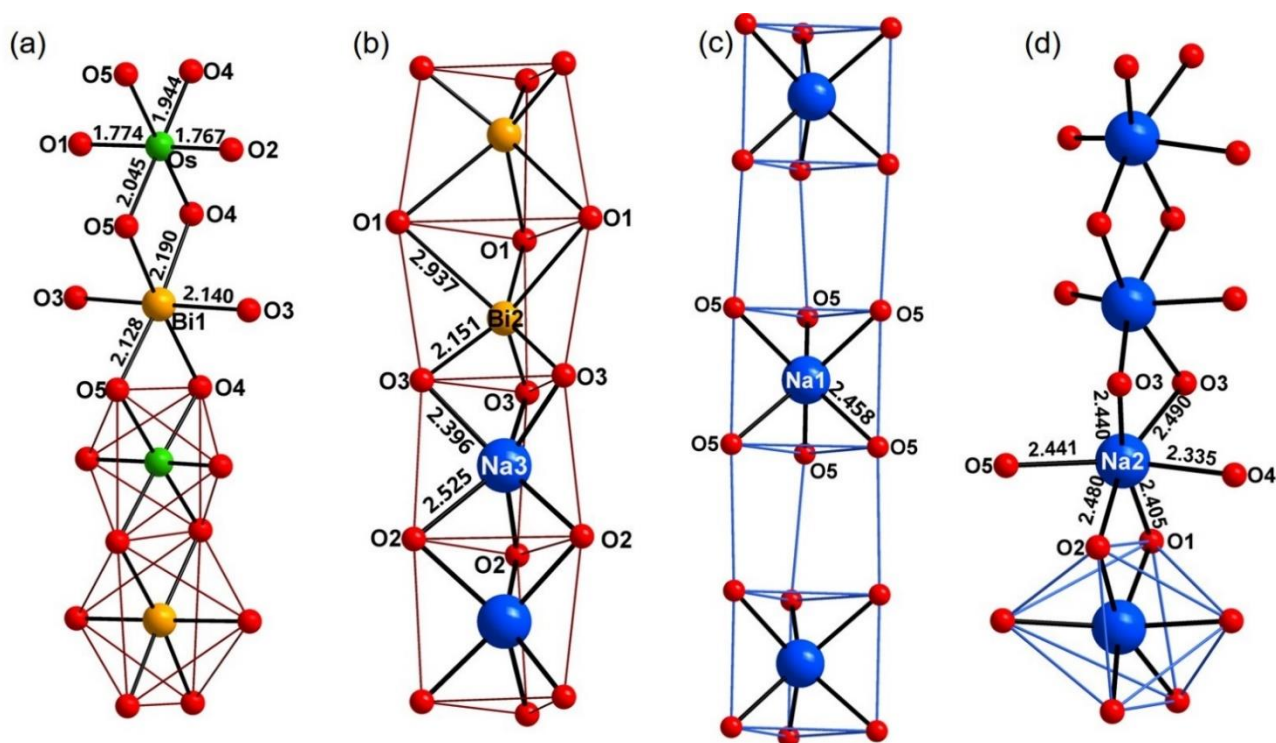


Figure 3. Presentation of the individual quasi-1D secondary building units, (a) chains of edge-shared alternating Os/Bi octahedra, (b) chains of alternating pairs of trigonal prisms of Na3/Bi2, (c) chains of alternating empty and filled (Na1)O₆ trigonal prisms and (d) chains of edge shared distorted (Na2)O₆ octahedra, for details compare text. Bond lengths are in Å.

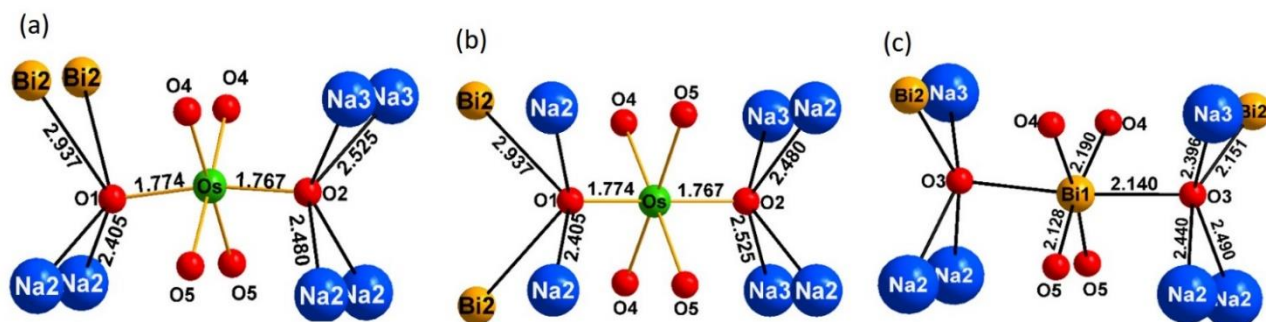


Figure 4. First coordination spheres of osmium(VI), (a) view direction perpendicular to, (b) within the crystallographic mirror plane, and (c) of bismuth(V). For osmium, the apical oxygen atoms are in a different local environment, generating local dipole moments, which completely compensate due to space group symmetry. Bond lengths are in Å

As one of the peculiar characteristics of the crystal structure found, cations as different as Bi³⁺ and Na⁺ (Bi2 and Na3) are hosted in virtually the same kind of trigonal prisms, see Figure 3b. Since this might cause some anti-site disorder between these two positions, we refined the respective site occupation factors. Indeed, slight indications were obtained for a low degree of anti-site disorder, exclusively for these two positions. The site occupation factor (SOF) of 96.53 and 3.47 (%) obtained is at the limits of experimental reliability, since SOF and temperature parameters are commonly strongly correlated in the refinements. This finding does not question the characteristics of the

crystal structure, in particular not the short bonds between osmium and the apical oxygen atoms, since the anti-site disorder only inverts the two different surroundings of the apical oxygen atoms. At screening crystals from different batches we became aware that this disorder may vary from one synthesis batch to the other, depending on the temperature schedules applied. At the extreme, SOF of 39.58% to 60.42% was encountered. Data of the split atom refinements are included in SI as Tables S5 – S9. The crystallographic data have been deposited at ICSD under CSD-No. 2063725 and 2063497, respectively.

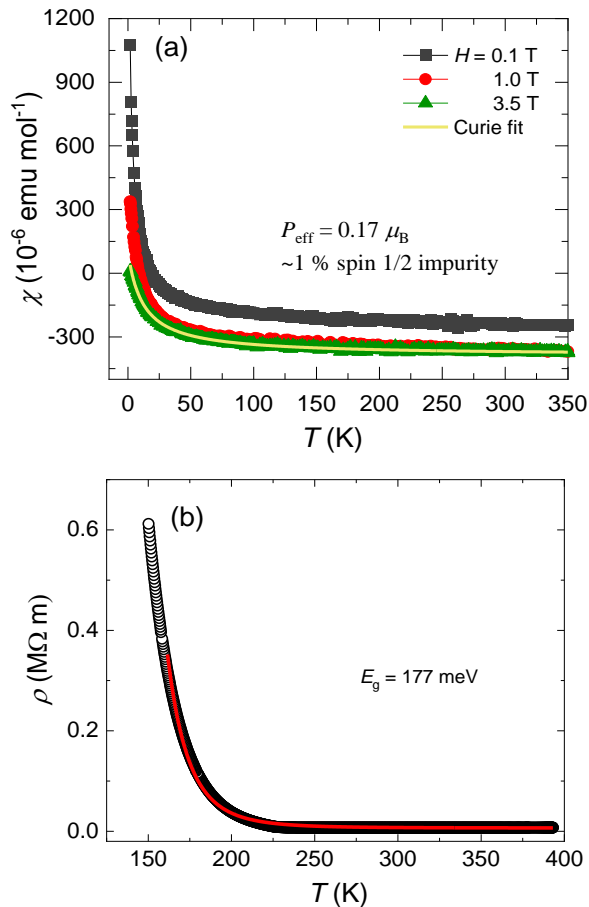


Figure 5. Temperature dependent magnetic susceptibility and its Curie fit ($\chi = C/T$) (a) and Arrhenius fit of electrical resistivity (b) of $\text{Na}_9\text{Bi}_5\text{Os}_3\text{O}_{24}$ single crystal(s).

The oxygen atoms constituting the smaller triangles are giving space to Bi^{5+} to adopt a virtually regular octahedron, while the wider triangles enable Os^{6+} to develop the strikingly short bonds to the apical oxygen atoms, i.e. to form a substantially compressed octahedron. Interestingly, this contraction is not forced by any matrix effect of the crystal structure. From Figure 4 one can see that there is sufficient freedom within the linkages Os-O1-Bi2 and Os-O2-Na3 to shift the respective oxygen atoms away from osmium. Even in the extreme, when moving O2 into the barycenter of the quadrilateral formed by Na2(2 \times) and Na3(2 \times), the Na-O separations are still within the common limit, see Figure S3. Thus, from a crystal chemistry point of view, there must be local electronic effects that are driving osmium into that peculiar configuration found experimentally.

Physical properties. Figure 5(a) shows the magnetic susceptibility carried out in the temperature range of 2-350 K at different applied magnetic fields (0.1, 1.0, 3.5 T), clearly indicating

the diamagnetic nature of the sample. Minor Curie tailing observed at low temperatures corresponds to an upper estimate of a magnetic moment $P_{\text{eff}} = 0.17 \mu_B/\text{mol}$ corresponding to 1 % of a spin $1/2$ impurity (from a Curie fit of the susceptibility in the entire temperature range). Electrical resistivity data (Figure 5b) shows that the compound is semiconducting with a band gap of 177 meV.

Computational results, theoretical analyses. In order to uncover the physical origin of the low-spin state stabilization in $\text{Na}_9\text{Bi}_5\text{Os}_3\text{O}_{24}$ we calculated the crystal-field splitting of the Os t_{2g} sub-shell in the DFT approach (see Figure 6) and found that it amounts to 1.4 eV, with the singlet xy orbital lying below the doublet xz, yz (in the local coordinate system with axes directed from Os towards oxygen atoms, z direction to the apical ligands). This separation virtually corresponds by magnitude to the $t_{2g}-e_g$ splitting ($10Dq$) in conventional $3d$ transition metal oxides. Considering Hund's energy for $5d$ ions of $\sim 0.5 \text{ eV}$,²² it is well understandable that the lowest xy orbital is filled by two electrons of Os^{6+} , resulting in a singlet ground state, $S=0$. Thus, it is clearly the strong crystal-field (ratio of short and long Os-O bonds is ~ 0.89), which leads to the non-magnetic state in the investigated material. It is worthwhile mentioning that, based on various experimental evidences, there have been claims of a low-spin state realized in t_{2g} configurations.⁶ However, respective theoretical and experimental studies did not confirm such a picture, see^{7,22} and references therein. To the best of our knowledge $\text{Na}_9\text{Bi}_5\text{Os}_3\text{O}_{24}$ is thus the only oxide, where such a situation affecting a set of t_{2g} levels is actually realized.

For checking the role of the degree of filling of the $5d$ derived states, we performed crystal structure optimizations with an artificially reduced number of electrons in the system of six per formula unit (compensated by a corresponding surrounding charge) or by substituting W^{6+} ($5d^0$) for Os^{6+} (volume, unit cell shape, atomic positions were allowed to relax). The results are qualitatively similar and rather illustrative. In the first case, of reduced number of electrons, the distance from the plane formed by equatorial oxygen atoms to apical ligands increases (1.87 and 1.97 Å), while the in-plane M-O bond lengths decrease (1.87 Å(2 \times) and 1.89 Å(2 \times)), for positional parameters see Table S10 in SI. When giving the $5d^2$ electrons back to the system (or reinstating Os for W), the structure returns to the original experimental configuration upon computational relaxation. These observations clearly demonstrate that the compression of the OsO_6 octahedron is basically caused by electronic effects, i.e. is due to a JT effect lifting the t_{2g} orbital degeneracy.

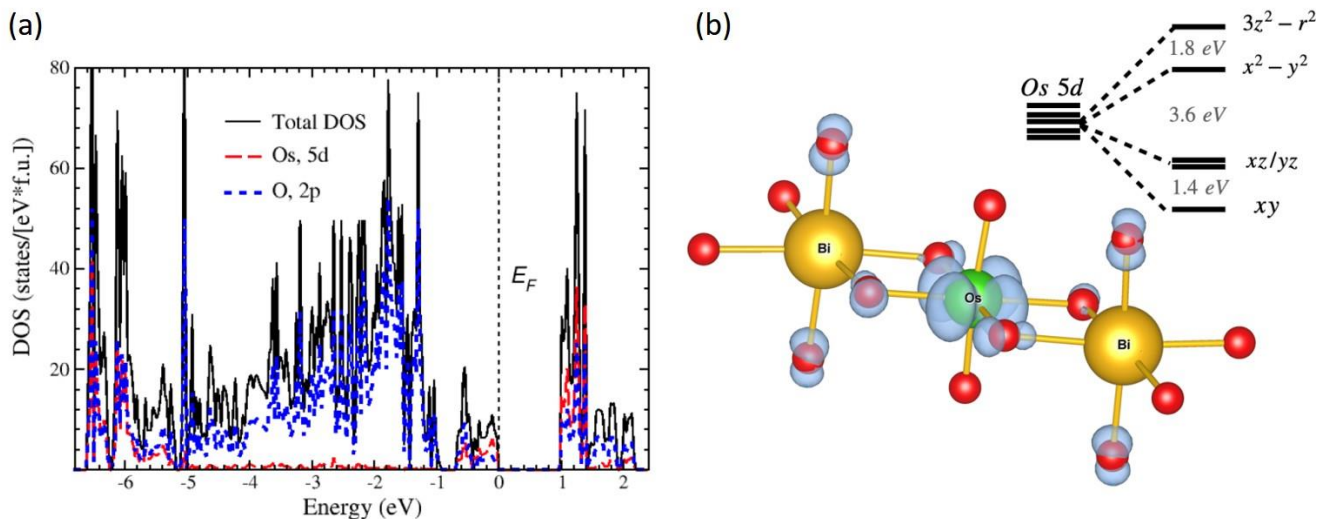


Figure 6. Total and partial density of states plots (a) and charge density (blue) corresponding to a single occupied band (just below the Fermi level, see left panel) in the GGA+U calculation (b). This band has predominantly Os d states character. Osmium (oxygen) atoms are shown by green (red) balls. Inset of (b) shows Os $5d$ level scheme.

It appears advisable to compare the situation in $\text{Na}_9\text{Bi}_5\text{Os}_3\text{O}_{24}$ with other functional oxides containing Os^{6+} . In principle, open shell $5d$ systems can arrive at a nonmagnetic state due to strong spin-orbit interaction even for a cubic crystal field. This has been encountered for $5d^4$ ions like Ir^{5+} .^{23,24} Also for Os^{6+} ($5d^2$) a nonmagnetic ground state owing to a combined action of spin-orbit coupling and cubic crystal field ($10 Dq$) has been reported.²⁵⁻²⁷ The character of this state, however, is very different from what we have in $\text{Na}_9\text{Bi}_5\text{Os}_3\text{O}_{24}$: it is not a singlet state with $S=0$, but a non-Kramers e_g doublet. Such an electronic state gives rise to low-lying magnetic states (for double perovskites like Ba_2MOsO_6 , $M=\text{Ca}, \text{Mg}, \text{Zn}$ the singlet-triplet gap is estimated as ~ 25 meV).²⁵ This would give strong and temperature-dependent van Vleck paramagnetism. In our case the situation is fundamentally different: there is a singlet state of Os^{6+} with $S=0$, with the gap to the lowest-lying magnetic state ($\Delta_{CF} - J_{Hund}$) = ~ 1 eV. Spin-orbit coupling plays practically no role in its stabilization. DFT+U+SOC calculations fully support this conclusion. The orbital moment was found to be extremely small, $\sim 10^{-3} \mu_B$.

CONCLUSIONS

We report on new $\text{Na}_9\text{Bi}_5\text{Os}_3\text{O}_{24}$ which features a unique crystal structure and an unparalleled electronic ground state: an extremely compressed octahedron of the oxygen atoms coordinating osmium(VI) is giving rise to a nonmagnetic configuration by hosting the $5d^2$ electrons paired in the d_{xy} derived state. The splitting of the t_{2g} levels amounts to 1.4 eV, substantially surpassing the Hund's coupling energy for $5d$ ions of ~ 0.5 eV. This kind of a giant JT distortion, which is without precedent, is not enforced by structural matrix effects: the structure would offer sufficient space to enable a virtually regular octahedron without causing strain. Apparently, the energy landscape of configurations for $5d^2$ systems, like Os^{6+} , in approximately octahedral coordination by oxygen is rather flat and, depending on the balance of local electronic factors of

influence vs. structural constraints, diverse ground states may develop. Against this background it appears rewarding to inspect this kind of competing impacts, structural frustration vs. strive for an as low as possible local electronic state, on the basis of the structure type presented, which offers plenty of options for modifying the relevant conditions by aliovalent or isovalent substitution of any of the cations present. Such computational studies, at best followed by experimental validation, would have the potential to provide valuable insights in the hierarchy of perturbations defining the ground states of open shell transition element compounds.

ASSOCIATED CONTENT

Supporting Information. Results of quantitative analysis (EDS and wet chemical), thermal decomposition profile, additional structure figures, tables for crystallographic data, atomic coordinates, bond distances and anisotropic displacement parameters. "This material is available free of charge via the Internet at <http://pubs.acs.org>."

AUTHOR INFORMATION

Corresponding Author

* Prof. Dr. Martin Jansen
Email: m.jansen@fkf.mpg.de

Author Contributions

All authors have given approval to the final version of the manuscript.

ACKNOWLEDGMENT

G.S.T. thank the Cluster of Excellence *ct.qmat* (EXC 2147) funded by the Deutsche Forschungsgemeinschaft (DFG) for partial support. A.V.U. is grateful to the Quantum project (AAAA-A18-118020190095-4). The work of D. Kh. was funded by the DFG

(German Research Foundation) - Project number 277146847 - CRC 1238. DFT+U calculations (S.V.S.) were supported by the Russian Science Foundation via RSF-20-62-46047 project.

REFERENCES

- (1) Wedig, U.; Jansen, M. A Piece of the Picture – Misunderstanding of Chemical Concepts. *Angew. Chem. Int. Ed.* **2008**, *47*, 10026–10029.
- (2) Shannon, R. D.; Prewitt, C. T. Effective Ionic Radii in Oxides and Fluorides. *Acta Crystallogr., Sect. B: Struct. Crystallogr. Cryst. Chem.* **1969**, *25*, 925–946.
- (3) Pauling, L. The Nature of the Chemical Bond. IV. The Energy of Single Bonds and the Relative Electronegativity of Atoms. *J. Am. Chem. Soc.* **1932**, *54*, 3570–3582.
- (4) Jensen, W. B. The origin of the oxidation-state concept. *J. Chem. Educ.* **2007**, *84*, 1418–1419.
- (5) Selwood, P. W. Magnetochemistry, Interscience publishers, New York, **1956**.
- (6) Khalifah, P.; Osborn, R.; Huang, Q.; Zandbergen, H. W.; Jin, R.; Liu, Y.; Mandrus, D.; Cava, R. J. Orbital ordering transition in $\text{La}_4\text{Ru}_2\text{O}_{10}$. *Science*, **2002**, *297*, 2237–2240.
- (7) Wu, H.; Hu, Z.; Burnus, T.; Denlinger, J. D.; Khalifah, P. G.; Mandrus, D.; Jang, L. -Y.; Hsieh, H. H.; Tanaka, A.; Liang, K. S.; Allen, J. W.; Cava, R. J.; Khomskii, D. I.; Tjeng, L. H.; Orbital driven spin-singlet dimerization in $S = 1$ $\text{La}_4\text{Ru}_2\text{O}_{10}$. *Phys. Rev. Lett.* **2006**, *96*, 256402.
- (8) Bruker **2017**. TOPAS Version 6, Bruker AXS, Karlsruhe, Germany.
- (9) Oszlányi, G.; Süto, A. Ab initio structure solution by charge flipping. *Acta Cryst.* **2004**, *A60*, 134–141.
- (10) Karle, J.; Hauptman, H. A theory of phase determination for the four types of non-centrosymmetric space groups $1P222$, $2P22$, $3P12$, $3P22$. *Acta Cryst.* **1956**, *9*, 635–651.
- (11) Bruker Suite, version 2013/1. Bruker AXS Inc., Madison, WI, **2013**.
- (12) SADABS — Bruker AXS area detector scaling and absorption, version 2016/2, Krause L.; Herbst-Irmer, R.; Sheldrick, G. M. *J. Appl. Cryst.* **2015**, *48*, 3–10.
- (13) Sheldrick, G. M. A Short History of SHELX. *Acta Crystallogr., Sect. A: Found. Crystallogr.* **2008**, *64*, 112–122.
- (14) Sheldrick, G. M. Crystal Structure Refinement with SHELXL. *Acta Crystallogr., Sect. C: Struct. Chem.* **2015**, *71*, 3–8.
- (15) Perdew, J. P.; Burke, K.; Ernzerhof, M. Generalized Gradient Approximation Made Simple. *Phys. Rev. Lett.* **1996**, *77*, 3865.
- (16) Mosca, D. F.; Pourovskii, L. V.; Kim, B. H.; Liu, P.; Sanna, S.; Boscherini, F.; Khmelevskiy, S.; Franchini, C. Interplay between Multipolar Spin Interactions, Jahn-Teller Effect and Electronic Correlation in a $J_{\text{eff}} = 3/2$ Insulator. Accepted, *Phys. Rev. B*, **2021**, <http://arxiv.org/abs/2102.10839>.
- (17) Andersen, O. K.; Jepsen, O. Explicit, First-Principles Tight-Binding Theory. *Phys. Rev. Lett.* **1984**, *53*, 2571.
- (18) O'Keeffe, M.; Andersson, S. Rod Packings and Crystal Chemistry. *Acta Cryst.* **1977**, *A33*, 914–923.
- (19) Andersson, S. On the Description of Complex Inorganic Crystal Structures. *Angew. Chem. Int. Ed. Engl.* **1983**, *22*, 69–81.
- (20) Stoltzfus, M. W.; Woodward, P. M.; Seshadri, R.; Klepeis, J.-H.; Bursten, B. Structure and Bonding in SnWO_4 , PbWO_4 , and BiVO_4 : Lone Pairs vs Inert Pairs. *Inorg. Chem.* **2007**, *46*, 3839–3850.
- (21) Fischer, R. C.; Power, P. P. π -Bonding and the Lone Pair Effect in Multiple Bonds Involving Heavier MainGroup Elements: Developments in the New Millennium. *Chem. Rev.* **2010**, *110*, 3877–3923.
- (22) Streltsov, S. V.; Khomskii, D. I. Orbital Physics in Transition Metal Compounds: New Trends. *Phys. -Usp.* **2017**, *60*, 1121–1146.
- (23) Prasad, B. E.; Doert, Th.; Felser, C.; Jansen, M. On $J_{\text{eff}} = 0$ Ground State Iridates(V): Tracking Residual Paramagnetism in New $\text{Bi}_2\text{NaIrO}_6$. *Chemistry, a Europ. J.* **2018**, *24*, 16762–16765.
- (24) Streltsov, S. V.; Khomskii, D. I. Jahn-Teller Effect and Spin-Orbit Coupling: Friends or Foes? *Phys. Rev. X* **2020**, *10*, 031043.
- (25) Paramakanti, A.; Maharaj, D. D.; Gaulin, B. D. Octupolar Order in D-Orbital Mott Insulators. *Phys. Rev. B* **2020**, *101* (5), 054439.
- (26) Maharaj, D. D.; Sala, G.; Stone, M. B.; Kermarrec, E.; Ritter, C.; Fauth, F.; Marjerrison, C. A.; Greedan, J. E.; Paramakanti, A.; Gaulin, B. D. Octupolar versus Néel Order in Cubic $5d^2$ Double Perovskites. *Phys. Rev. Lett.* **2020**, *124*, 87206.
- (27) Voleti, S.; Maharaj, D. D.; Gaulin, B. D.; Luke, G.; Paramakanti, A. Multipolar Magnetism in D-Orbital Systems: Crystal Field Levels, Octupolar Order, and Orbital Loop Currents. *Phys. Rev. B* **2020**, *101*, 155118.

Supplementary Material

Na₉Bi₅Os₃O₂₄: A Unique Diamagnetic Oxide Featuring a Pronouncedly Jahn-Teller Compressed Octahedral Coordination of Osmium(VI)

Gohil S. Thakur,^{1,2} Hans Reuter,³ Alexey V. Ushakov,⁴ Gianpiero Gallo,⁵ Jürgen Nuss,⁵ Robert E. Dinnebier,⁵ Sergey V. Streltsov,⁴ Daniel I. Khomskii,⁶ and Martin Jansen^{5*}

Contents:

1. Quantitative analysis using SEM-EDX
2. Thermal decomposition profile
3. Additional structures sections from experiment and DFT calculations
4. Results of chemical analysis
5. Tables of atomic coordinates, bond lengths and thermal parameter

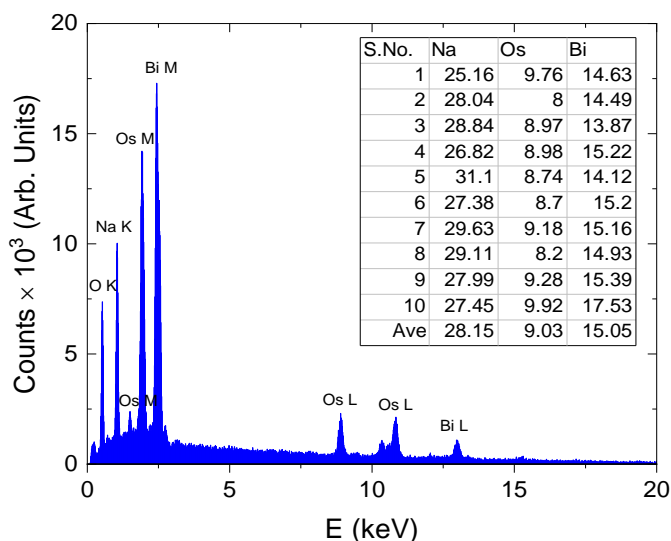


Figure S1: Elemental analysis of a typical crystal of Na₉Bi₅Os₃O₂₄ using SEM-EDX. Inset shows table of atomic ratios at different regions.

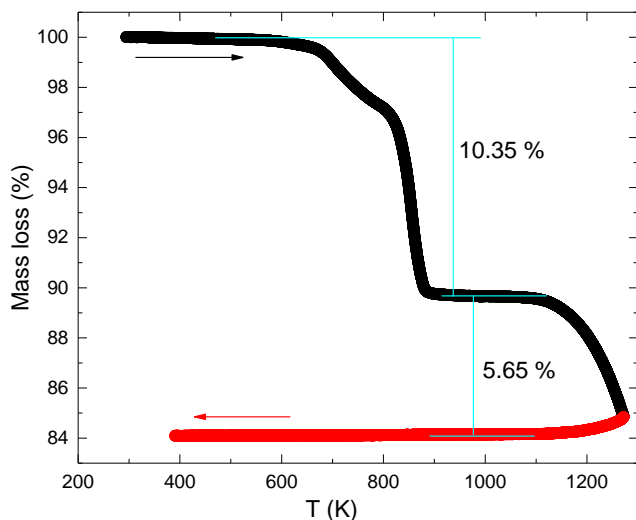


Figure S2. Thermal decomposition profile of $\text{Na}_9\text{Bi}_5\text{Os}_3\text{O}_{24}$.

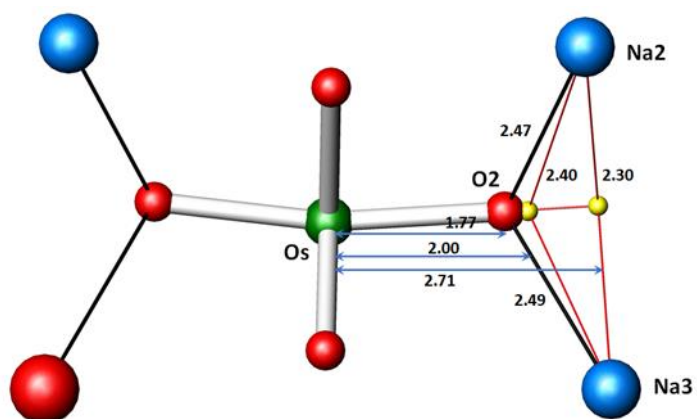


Figure S3. Demonstrating lack of structural frustration with respect to short apical Os-O2 bond. The distances are in Å.

Table S1. Wet chemical (ICP-OES/ AAS) analysis. Mole fraction is normalized to Os.

Atom	Mass % (1 run)	Mass % (2 run)	Average	Mole fraction	Normalized
Bi	46.5	46.4	46.45	0.2223	4.8
Na	9.34	8.98	9.16	0.3984	8.6
Os	26.5	26.2	26.35	0.1385	3.0
O (remaining)	17.66	18.42	18.04	1.128	24.4

Table S2: Atomic coordinates for $\text{Na}_9\text{Bi}_5\text{Os}_3\text{O}_{24}$ obtained by Rietveld refinement of room temperature powder data.

Atom	Wyck.	x	y	z
Os1	6h	0.66806	-0.0022	1/4
Bi1	6g	0.67116	0	1/2
Bi2	4f	1/3	2/3	0.606
Na1	2b	0	0	1/4

Na2	12i	0.29206	0.98487	0.37917
Na3	4f	1/3	2/3	0.39554
O1	6h	0.80232	0.1869	1/4
O2	6h	0.56344	0.79511	1/4
O3	12i	0.52977	0.75106	0.49004
O4	12i	0.52719	0.00702	0.37432
O5	12i	0.78861	0.99129	0.38295

Table S3: Selected bond distances obtained for Na₉Bi₅Os₃O₂₄ obtained by Rietveld refinement.

Atom pairs	Distance (Å)	Atom pairs	Distance (Å)
Os1-O1 (×1)	1.656	Na1-O5 (×6)	2.658
Os1-O2 (×1)	1.725		
Os1-O5 (×2)	2.099	Na2-O4 (×1)	2.211
Os1-O4 (×2)	2.146	Na2-O3 (×1)	2.337
		Na2-O5 (×1)	2.453
Bi1-O5 (×2)	1.925	Na2-O1 (×1)	2.461
Bi1-O3 (×2)	2.129	Na2-O2 (×1)	2.490
Bi1-O4 (×2)	2.171	Na2-O3 (×1)	2.688
Bi2-O3 (×3)	2.243	Na3-O3 (×3)	2.071
Bi2-O4 (×3)	2.798	Na3-O2 (×3)	2.711

Table S4: Anisotropic displacement parameters ($\text{Å}^2 \times 10^3$) for Na₉Bi₅Os₃O₂₄, ordered structure model. The anisotropic displacement factor exponent takes the form: $-2\pi^2[h^2a^{*2}U_{11} + \dots + 2hka^*b^*U_{12}]$.

Atom	U11	U22	U33	U23	U13	U12
Os	5(1)	5(1)	2(1)	0	0	2(1)
Bi1	6(1)	5(1)	2(1)	0(1)	0(1)	2(1)
Bi2	9(1)	9(1)	5(1)	0	0	4(1)
Na1	15(2)	15(2)	20(3)	0	0	7(1)
Na2	9(1)	14(2)	12(2)	1(1)	0(1)	3(1)
Na3	3(1)	3(1)	43(4)	0	0	1(1)
O1	14(4)	3(3)	9(2)	0	0	2(2)
O2	15(3)	2(3)	9(2)	0	0	1(3)
O3	9(2)	5(2)	8(2)	1(2)	2(2)	4(2)
O4	6(2)	14(2)	6(2)	-1(2)	1(2)	6(2)
O5	9(2)	14(2)	4(2)	1(2)	0(2)	7(2)

Table S5: Crystal data and structure refinement for Na₉Bi^V₃Bi^{III}₂Os₃O₂₄.

Crystal	1	2
Identification code	HR2212_0m	nus313a_0m
Empirical formula	Bi ₅ Na ₉ O ₂₄ Os ₃	
Formula weight [g/mol]	2206.41	
T [K]	296(2)	

Crystal data			
Crystal system, space group	Hexagonal, $P\bar{6}2c$		
a [Å]	9.8115(3)		9.8344(2)
c [Å]	12.8457(5)		12.8732(5)
V [Å ³]	1070.93(8)		1078.23(6)
Z, d _{calc} [g/cm ³]	2, 6.842		2, 6.796
μ (MoK α) [mm ⁻¹]	58,944		58,545
F(000)	1868		
Data collection			
2 θ _{max}	70°		
Reflections collected	75234		18635
Reflections unique, R _{int}	1637, 0.0877		1639, 0.0508
Refinement			
Data / restraints / parameters	1637 / 0 / 70	1637 / 0 / 75	1639 / 0 / 76
Goodness-of-fit on F ²	1,040	1,037	1,055
R ₁ , wR2 [I > 2s(I)]	0.0208, 0.0529	0.0176, 0.0421	0.0242, 0.0911
R ₁ , wR2 [all data]	0.0268, 0.0567	0.0234, 0.0451	0.0288, 0.0965
Absolute structure parameter	-0.038(6)	-0.033(11)	0.024(11)
Extinction coefficient	0.00102(5)	0.00144(6)	0.00076(10)
$\pm D$ [eÅ ⁻³]	1.729/-3.396	1.728/-1.905	2.687/-3.289
Structure model			
Na/Bi-disorder	no	yes	yes
Degree of anti-site disorder	0%	96.53%/3.47%	39.58%/60.42%

Table S6. Atomic coordinates ($\times 10^4$) and equivalent isotropic displacement parameters ($\text{Å}^2 \times 10^3$) for crystal 1 and 2 of Na₉Bi₅Os₃O₂₄ obtained after refinement (top rows) and with anti-site disorder (bottom rows). U(eq) is defined as one third of the trace of the orthogonalized U_{ij} tensor.

Atom	Sample	Bi/Na-disorder	Wyckoff	Occ.	x	y	z	U(eq)
Os	1	no	6h		6682(1)	9975(1)	2500	4(1)
	1	yes			6682(1)	9975(1)	2500	5(1)
	2	yes			3300(1)	-8(1)	2500	9(1)
Bi1	1	no	6g		6712(1)	10000	5000	5(1)
	1	yes			6711(1)	10000	5000	5(1)
	2	yes			3294(1)	0	5000	10(1)
Bi2A	1	no	4f		3333	6667	6051(1)	7(1)
	1	yes		0.965(3)	3333	6667	6051(1)	7(1)
	2	yes		0.396(3)	6667	3333	3961(1)	16(1)
Bi2B	1	no						

	1	yes	4f	0.035	3333	6667	3997(11)	11(3)
	2	yes		0.604	6667	3333	6043(1)	10(1)
Na1	1	no	2b		10000	10000	2500	17(1)
	1	yes			10000	10000	2500	19(1)
	2	yes			0	0	7500	28(2)
Na2	1	no	12i		2976(6)	9912(4)	3789(2)	13(1)
	1	yes			2994(5)	9916(3)	3788(2)	13(1)
	2	yes			6949(8)	-24(4)	6211(3)	20(1)
Na3A	1	no	4f		3333	6667	3731(4)	16(1)
	1	yes		0.965(3)	3333	6667	3654(6)	19(2)
	2	yes		0.396(3)	6667	3333	6370(20)	57(13)
Na3B	1							
	1	yes	4f	0.035	3333	6667	6440(140)	19(2)
	2	yes		0.604	6667	3333	3581(15)	47(6)
O1	1	no	6h		8035(13)	12028(12)	2500	10(1)
	1	yes			8032(12)	12026(11)	2500	12(1)
	2	yes			2159(18)	-2079(15)	7500	22(2)
O2	1	no	6h		5648(8)	7895(11)	2500	10(1)
	1	yes			5649(7)	7892(10)	2500	12(1)
	2	yes			4127(11)	2040(14)	7500	22(2)
O3	1	no	12i		5336(5)	7486(6)	5037(3)	7(1)
	1	yes			5337(5)	7490(5)	5037(3)	9(1)
	2	yes			4649(6)	2510(6)	5010(4)	11(1)
O4	1	no	12i		5443(6)	10117(6)	3631(4)	8(1)
	1	yes			5443(5)	10119(5)	3632(3)	10(1)
	2	yes			4624(7)	32(8)	6365(5)	18(1)
O5	1	no	12i		7987(7)	9862(7)	3703(4)	8(1)
	1	yes			7983(6)	9859(6)	3703(3)	10(1)
	2	yes			1925(8)	-36(8)	6290(4)	17(1)

Table S7. Summary of bond lengths [Å] obtained from single crystal structure refinement using different protocols of refinement for all crystal samples

Crystal	1	1	2
Na/Bi-disorder	no	yes	yes
Degree of disorder	0%	96.53%/3.47%	39.58%/60.42
Os1-O2 (×1)	1.767(10)	1.770(9)	1.755(13)
Os1-O1 (×1)	1.773(11)	1.771(10)	1.767(14)
Os1-O4 (×2)	1.944(5)	1.945(4)	1.944(6)
Os1-O5 (×2)	2.044(5)	2.043(4)	2.054(6)
Bi1-O5 (×2)	2.129(5)	2.128(4)	2.126(6)
Bi1-O3 (×2)	2.140(5)	2.136(4)	2.140(5)
Bi1-O4 (×2)	2.191(5)	2.190(4)	2.182(6)
Bi2A-O3 (×3)	2.150(5)	2.151(4)	2.193(5)
Bi2B-O3 (×3)		2.172(10)	2.180(5)

Na1-O5 (×6)	2.457(5)	2.459(4)	2.466(7)
Na2-O4 (×1)	2.335(7)	2.319(6)	2.323(10)
Na2-O1 (×1)	2.406(9)	2.404(8)	2.465(12)
Na2-O3 (×1)	2.440(6)	2.440(5)	2.463(7)
Na2-O5 (×1)	2.441(7)	2.453(6)	2.580(9)
Na2-O2 (×1)	2.480(8)	2.478(7)	2.447(12)
Na2-O3 (×1)	2.490(6)	2.487(5)	2.450(6)
Na2-O5 (×1)			2.667(9)
Na3A-O2 (×3)	2.396(6)	2.464(6)	2.608(18)
Na3A-O3 (×3)	2.525(6)	2.467(7)	2.46(2)
Na3B-O3 (×3)		2.49(13)	2.524(15)
Na3B-O1 (×3)		2.65(9)	2.493(13)
		= Affected by disorder	

Table S8. Anisotropic displacement parameters ($\text{\AA}^2 \times 10^3$) for $\text{Na}_9\text{Bi}_5\text{Os}_3\text{O}_{24}$ assuming anti-site disorder (crystal 1). The anisotropic displacement factor exponent takes the form: $-2\pi^2[h^2a^{*2}U_{11} + \dots + 2hka^*b^*U_{12}]$

Atom	U11	U22	U33	U23	U13	U12
Os1	6(1)	5(1)	3(1)	0	0	3(1)
Bi1	7(1)	6(1)	3(1)	0(1)	0(1)	3(1)
Bi2A	9(1)	9(1)	5(1)	0	0	4(1)
Bi2B	12(3)	12(3)	8(7)	0	0	6(2)
Na1	17(2)	17(2)	23(3)	0	0	9(1)
Na2	12(1)	12(2)	12(2)	0(1)	-1(1)	4(1)
Na3A	19(2)	19(2)	19(3)	0	0	10(1)
Na3B	19(2)	19(2)	19(3)	0	0	10(1)
O1	15(4)	6(3)	10(2)	0	0	3(2)
O2	17(3)	5(3)	10(2)	0	0	3(3)
O3	10(2)	7(2)	10(2)	1(2)	3(1)	4(2)
4O4	8(2)	15(2)	8(2)	-1(2)	0(1)	7(2)
O5	11(2)	16(2)	5(2)	1(2)	1(1)	8(2)

Table S9. Anisotropic displacement parameters ($\text{\AA}^2 \times 10^3$) for $\text{Na}_9\text{Bi}_5\text{Os}_3\text{O}_{24}$ assuming inversion and disorder (crystal 2). The anisotropic displacement factor exponent takes the form: $-2\pi^2[h^2a^{*2}U_{11} + \dots + 2hka^*b^*U_{12}]$

Atom	U11	U22	U33	U23	U13	U12
Os1	10(1)	10(1)	8(1)	0	0	5(1)
Bi1	12(1)	10(1)	8(1)	0(1)	0(1)	5(1)
Bi2A	16(1)	16(1)	16(1)	0	0	8(1)
Bi2B	12(1)	12(1)	9(1)	0	0	6(1)
Na1	21(2)	21(2)	43(5)	0	0	10(1)
Na2	21(2)	16(2)	22(2)	1(1)	0(1)	8(2)
Na3A	80(19)	80(19)	13(10)	0	0	40(10)
Na3B	62(9)	62(9)	15(6)	0	0	31(4)
O1	30(6)	11(4)	15(3)	0	0	3(3)
O2	37(4)	5(4)	16(3)	0	0	5(4)

O3	15(2)	5(2)	14(2)	0(2)	0(1)	5(2)
O4	15(3)	26(3)	15(2)	-1(2)	0(2)	13(2)
O5	18(3)	27(3)	9(2)	1(2)	1(2)	14(3)

Table S10. DFT+U optimized crystal structure (unit cell volume and shape, atomic positions were allowed to relax, number of electrons decreased by 2 per each Os (compensated by external charges). Space group: $P\bar{6}2c$, $a = 9.01577 \text{ \AA}$, $c = 12.38993 \text{ \AA}$.

Atom	Wyckoff	x	y	z
Os1	$6h$	0.66543	-0.02727	0.2500
Bi1	$6g$	0.66530)	0.0000	0.000
Bi2	$4f$	0.3333	0.6667	0.62392
Na1	$2b$	0.0000	0.0000	0.2500
Na2	$12i$	0.28790	-0.0023	0.37657
Na3	$4f$	0.3333	0.6667	0.37511
O1	$6h$	0.77653	0.24262	0.2500
O2	$61h$	0.54505	0.75121	0.2500
O3	$12i$	0.53331	0.73165	0.50826
O4	$12i$	0.52839	0.00057	0.35882
O5	$12l$	0.81560	0.00601	0.35957